The giant electrorheological effect in suspensions of nanoparticles

WEIJIA WEN[1], XIANXIANG HUANG[1], SHIHE YANG[2], KUNQUAN LU[3] AND PING SHENG*[1]

[1]Department of Physics and Institute of Nano Science and Technology, The Hong Kong University of Science and Technology, Clear Water Bay, Kowloon, Hong Kong, China
[2]Department of Chemistry and Institute of Nano Science and Technology, The Hong Kong University of Science and Technology, Clear Water Bay, Kowloon, Hong Kong, China
[3]Institute of Physics, Chinese Academy of Sciences, Beijing 100080, China
*e-mail: sheng@ust.hk

Published online: 5 October 2003; doi:10.1038/nmat993

Electrorheology (ER) denotes the control of a material's flow properties (rheology) through an electric field[1–10]. We have fabricated electrorheological suspensions of coated nanoparticles that show electrically controllable liquid–solid transitions. The solid state can reach a yield strength of 130 kPa, breaking the theoretical upper bound on conventional ER static yield stress that is derived on the general assumption that the dielectric and conductive responses of the component materials are linear. In this giant electrorheological (GER) effect, the static yield stress displays near-linear dependence on the electric field, in contrast to the quadratic variation usually observed[11–16]. Our GER suspensions show low current density over a wide temperature range of 10–120 °C, with a reversible response time of <10 ms. Finite-element simulations, based on the model of saturation surface polarization in the contact regions of neighbouring particles, yield predictions in excellent agreement with experiment.

Figure 1a is a transmission electron microscope (TEM) image of the GER particles. They have an average size of 50–70 nm, each with a surface coating of ~3–10 nm. An important feature of the GER suspension is its large dielectric constant, around 50–60 (at 10 Hz) over the temperature range of 10–120 °C for the dense samples (≥30% volume fraction of particles). Silicone oil has a dielectric constant of ~2, so this large value is attributed to the coated nanoparticle, whose effective dielectric constant is dominated by its coating. Urea is known to have a large molecular dipole moment of $\mu = 4.6$ debye (and molecular number density of 1.3×10^{22} cm^{-3})[17]. An estimate of the polarizability $\alpha = \mu^2/3kT$ based on the free-dipole model, where k is the Boltzmann constant and T the temperature (300 K), yields a dielectric susceptibility $\chi \approx 5$ (with a molecular volume of ~100 Å^3), hence a dielectric constant $\varepsilon = 1 + 4\pi\chi \approx 60$ that is in reasonable agreement with the measured value. Thus thin urea coatings have a significant dielectric response due

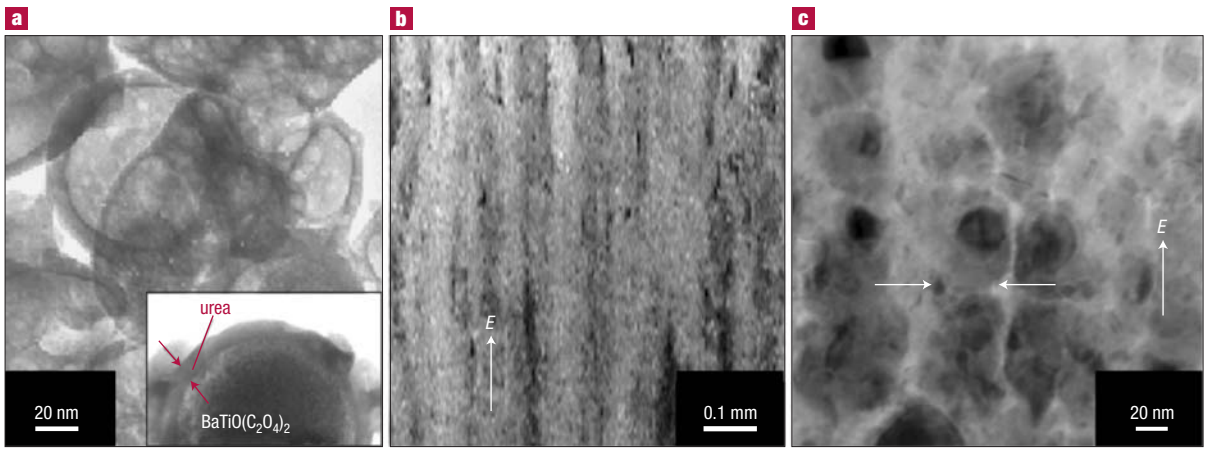

Figure 1 Images of nanoparticles in GER suspensions. a, TEM image of coated nanoparticles. Urea coatings are clearly seen. **b**, Optical microscope image of a sample prepared in epoxy, solidified under an applied field E of 2 kV mm^{-1}. Columns aligned along the field direction are visible. **c**, TEM image of a section of the column shown in **b**. The arrows indicate one of the flattened interfaces.

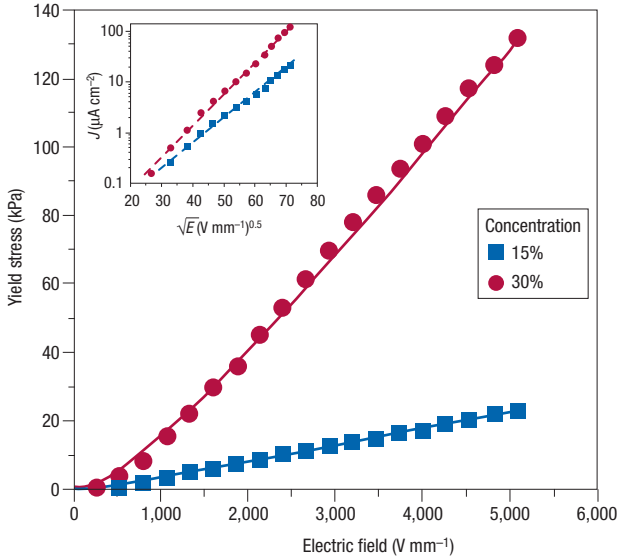

Figure 2 Static yield stress plotted as a function of applied electric field for two solid concentrations. Symbols denote experiment; solid lines are theory. Inset: logarithm of the current density J plotted as a function of $\sqrt{E}$. The dashed straight lines serve to delineate the relationship $\ln J \propto \sqrt{E}$, indicating the mechanism of activation over the Coulomb barrier.

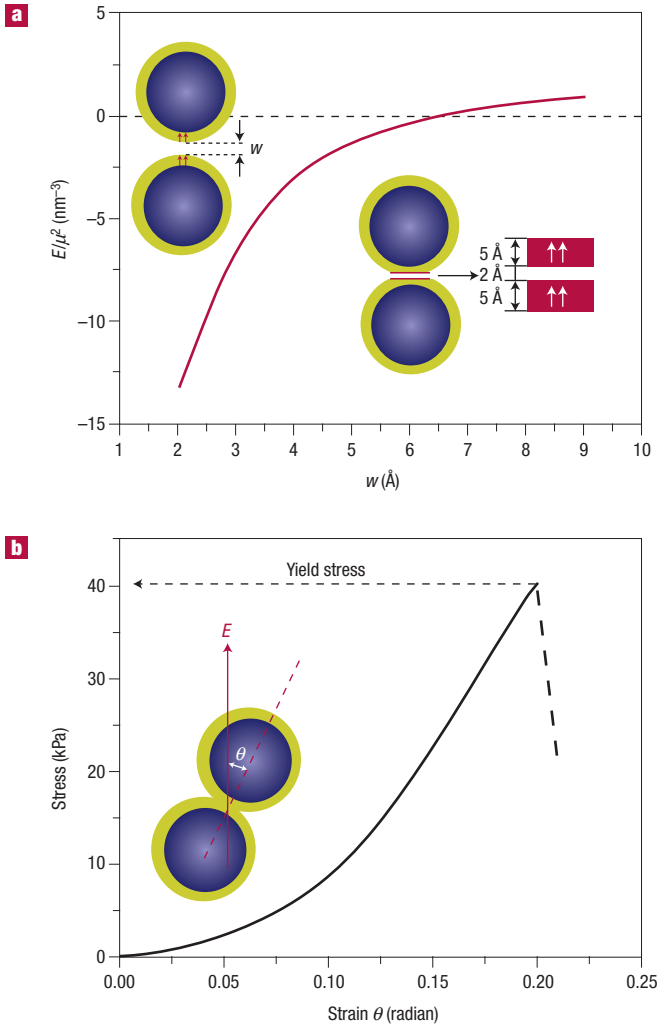

Figure 3 Illustration of the theoretical model with calculated results. a, Upper left: schematic picture of our model, consisting of two coated spheres, each with a 50-nm-diameter core and a 5-nm coating (both with $\varepsilon = 60$). The gap, with width w, has $\varepsilon = 2$ (for silicone oil). The solid curve shows the calculated interaction energy divided by μ^2 between two pairs of nearest-neighbour surface dipoles, each with $\mu = 4.6$ debye and separated laterally by 4.5 Å ($\varepsilon = 1$ between the dipoles), when w increases from 2 Å. Negative interaction energy indicates the aligned dipolar configuration to be favoured over the (random) non-aligned configuration. Lower right: the two spheres in elastic contact. An enlarged picture of the contact region shows a 2-Å gap (required by the steric repulsion between the molecules) sandwiched by two aligned dipolar layers. **b**, Calculated static stress–strain (θ) relation at 2 kV mm^{-1}. The static yield stress is the peak stress value, beyond which the stress decreases with increasing strain, indicated by the dashed line for instability. There is a discontinuity in the derivative at the yield point. At 2 kV mm^{-1}, the equilibrium elastic deformation ΔL is 1.2 nm, increasing to 2.2 nm at 5 kV mm^{-1}. The gap width was fixed at 2 Å for all calculations in which the spheres were in elastic contact.

to the existence of the interfaces. In particular, the short-range (other than dipolar) interactions between the coating molecules and the core (barium titanyl oxalate) particle, and/or the oil, must be such that the molecular dipoles are unlocked from antiparallel pairings (which would imply insensitivity to the external field and hence a small dielectric response).

Under an applied electric field, induced polarization in the particles causes their aggregation into columns aligned along the field direction (Fig. 1b). These columns are responsible for the solid yield stress when sheared perpendicular to the columns. A closer look at one of the columns is shown in Fig. 1c, where it is seen that the particles' contact areas are somewhat flattened, indicating a degree of softness in the coatings.

The static yield stress curves for two volume fractions, measured under d.c. electric fields, are shown in Fig. 2. The corresponding current densities are shown in the inset. The current density J is below 4 μA cm^{-2} at $E < 2$ kV mm^{-1} for the 30% sample. The yield stress varies as a function of temperature from 10 to 120 °C by no more than 30%. A similar temperature variation in current density was observed. At 1 kV mm^{-1} and 30% volume concentration, our GER has a measured Young's modulus $Y \approx 6$ MPa under pulling. At concentrations under 15%, both the onset and decay times of the yield stress are of the order of 10 ms. At high concentrations, however, the initial fast decay of the yield stress is usually accompanied by a long time tail (extending to ~1 s) that is small in magnitude, implying a degree of metastability.

The magnitude of the static yield stress for this GER fluid, reaching 130 kPa at 5 kV mm^{-1}, sets it apart from the conventional ER fluids because it exceeds the theoretical upper bound[15,18], $(138\sqrt{R})(\varepsilon_1 E^2/8\pi)$ (with R the particle radius in units of micrometres, and ε_1 denoting dielectric constant of the liquid), derived on the general assumption of linear dielectric and electrical conductive responses of the component materials. With $\varepsilon_1 = 2$ for the silicone oil dielectric constant, $R = 0.04$ (μm) and $E = 5$ kV mm^{-1}, the upper bound is 6.1 kPa, ~20 times smaller than the observed value. Another characteristic of GER is its near-linear field dependence of the yield stress. In general, the static yield stress is proportional to the energy density $-\mathbf{P}\cdot\mathbf{E}$, where $\mathbf{P}$ is the polarization density. A linear dependence of $\mathbf{P}$ on $\mathbf{E}$, that is, $\mathbf{P} = \chi\mathbf{E}$, implies a quadratic field dependence of the yield stress. The observed near-linear field dependence suggests the GER mechanism to involve a constant $\mathbf{P}_0$, that is, a saturation polarization.

It should be noted that the nonlinear conduction mechanism[19], based on the dissociation of fluid molecules under high electric field,

predicts[20] a non-parabolic $E^{3/2}$ dependence of the yield stress, with a maximum yield stress[20] (within reasonable parameter values) of ~25 kPa at 4 kV mm^{-1}, four times smaller than that observed in GER suspensions. Also, as we used the same silicone oil for suspensions of bare barium titanyl oxalate particles and coated particles, with the latter having an order of magnitude larger yield stress, we conclude that the coating, rather than the fluid, plays the crucial role in the GER effect.

We propose that saturation surface polarization, in the contact region of the neighbouring spheres, is responsible for the GER effect. In Fig. 3a we show a schematic picture of our model, consisting of two spherical coated particles with a flattened contact area. For the parameters of the model, see Fig. 3. The contact region is modelled by a 2-Å gap separating the two surfaces, with an area determined by the hertzian solution[21] of two elastic spheres pulled together by a force F. The area is $\pi F^{2/3}(\kappa R/2)^{2/3}$, where R denotes the coated sphere radius and κ^{-1}, the deformation modulus of the coating, is the only adjustable parameter of our model. In the contact region the surface dipoles form two aligned layers as shown in Fig. 3a, in contrast to other areas where such a configuration represents a higher energy state. The aligned configuration is possible because of (1) the high dielectric constant of the coating, which reduces the repulsive interaction between the aligned dipoles, (2) the favourable attractive interaction across the gap which considerably lowers the overall energy, and (3) the magnitude of the favourable interaction energy, which is sufficient to overcome the entropy effect. To buttress our argument, we have used a finite-element approach to calculate the interaction energy for two (nearest-neighbour) pairs of dipoles, shown schematically in Fig. 3a. The result shows that the interaction energy is lowered with decreasing gap separation (Fig. 3a) even in the absence of an applied field. Here zero means the unpolarized state (random orientations). The interaction energy at the gap separation of $w = 2$ Å is about $-7kT$, sufficient to overcome the entropy effect and to induce a localized collective transition to the aligned state. Thus when the two particles are pulled together under a moderate field, saturated surface polarization becomes the preferred configuration in the contact region.

To calculate the static yield stress, we used continuum electrostatics where the contact surfaces are decorated with a polarization density $P_0 = 4.6$ debye per 0.1 nm^3. The two spheres are sheared by an angle θ (relative to the applied field direction), and the total electrostatic energy difference ΔW_{es}, relative to the $\theta = 0$ state, is calculated under a fixed E. The electrostatic force pulling the two spheres together is $F = \mathrm{d}(\Delta W_{es})/\mathrm{d}(\Delta L)$, ΔL being the approach between the centres. The stress is obtained as $(\mathrm{d}\Delta W/\mathrm{d}\theta)_o/V$, where V is the average volume occupied by a coated sphere, $\Delta W = \Delta W_{es} + \Delta W_{elas}$, the latter being the elastic deformation energy difference (from the $\theta = 0$ state), and subscript o indicates the derivative to be evaluated at the equilibrium point. Shear strain is simply θ. The static yield stress is the maximum point in the stress–strain relation, beyond which the stress decreases as strain increases, indicating instability. This is identified in our model as the shear angle where the two spheres are barely touching. Shown in Fig. 3b is the calculated stress–strain relation for $E = 2$ kV mm^{-1}, with a deformation modulus, fitted to the experimental yield stress, of $\kappa^{-1} \approx 0.12$ GPa.

The predicted yield stress as a function of E is shown in Fig. 2 (solid lines). Excellent agreement between theory and experiment is seen. In particular, the discernable deviation from linearity is well captured by the elastic component of the model. For the 15% concentration, however, our model obtains agreement only by using a solid concentration of 5% (by using three times the average volume per particle than the 15% case). This is plausible because the theoretical concentration is that of the network backbone responsible for the overall rigidity; at lower concentrations the probability increases that a solid particle in the actual (random) system does not belong to the backbone. With no adjustable parameter, the Young's modulus $Y = [\mathrm{d}^2(\Delta W)/\mathrm{d}(\Delta L/L)^2]_o/V$ was calculated to be 5 MPa at 1 kV mm^{-1} for a concentration of 30%, in good agreement with experiment (6 MPa).

The conduction current density in polar ER fluids is attributed to the thermal generation of charge carriers when ions, possibly originating from the molecular dipoles, are activated over the Coulomb barrier from the counter-ions. A signature of such activation is the lowering of the Coulomb barrier as $\sqrt{E}$ (refs 22, 23). In Fig. 2 we show that $\ln J \propto \sqrt{E}$, confirming this physical picture. Breakdown occurs when current heating induces a thermal runaway. Our GER colloids could potentially function as an interface that translates electrical signals into mechanical signals, opening the possibility of actively controllable clutches, dampers, valves and locks[24].

METHODS

SAMPLE PREPARATION

The GER particles were fabricated by first dissolving barium chloride in distilled water[25,26] at 50–70 °C. Separately, oxalic acid was dissolved in water at 65 °C in an ultrasonic tank, with titanium tetrachloride slowly added. The two solutions were mixed in an ultrasonic bath at 65 °C. Nanometre-sized barium titanyl oxalate particles were formed at this stage. X-ray characterization showed the particles to be amorphous in structure. These bare particles, when mixed with silicone oil, have a maximum static ER yield stress of the order of 5 kPa. Addition of urea to the mixed solution led to the formation of a white colloid, which was cooled to room temperature. The precipitate was washed with water, filtered, and then dried to remove all trace water. The dried white powder consisted of the nanoparticles coated with urea, that is, $(BaTiO(C_2O_4)_2 + NH_2CONH_2)$. In such a core/shell structure (Fig. 1a), urea serves as an ER promoter. Here the urea could be replaced with other chemicals, such as acrylamide. We prepared ER fluids by mixing the powder with silicone oil and homogenizing it in a high-speed grinding mill for ~2 hours. The sample was then vacuum-dried at 105–120 °C for 1–3 hours. The final suspension is stable, with no observable sedimentation after a few weeks on the shelf.

DATA COLLECTION

In this work the solid volume fraction was calculated on the basis of the core (barium titanyl oxalate) particle weight and density. This volume fraction should be regarded as an underestimate, as it excludes the coatings. From the dielectric constant and inferred elastic deformation of the coated particles, there are reasons to believe that the urea coatings have different physical characteristics from bulk urea. The rheological properties were measured by a circular-plate type viscometer (Haake RS1, 8 mm in diameter) with a gap width of 1 mm, under d.c. applied voltage. We used a PM5134 (Philips) functional generator to generate linear and step signals for driving the d.c. high-voltage source (SPELLMAN SL300). Temperature was controlled with an oil bath tank (Thermo Haaka). Experimental data were collected with the help of the software package Rheowin. The electric field was applied to the GER colloid sandwiched between two parallel plates. Two approaches were used to measure the static yield stress. In the first approach we chose the controlled stress (CS) mode of operation, in which the deformation was monitored while the stress was continuously increased. The static yield stress was determined by the maximum shear stress value at which a kink occurs in the strain–stress curve, beyond which the strain increases almost vertically. In the second approach the shear rate was varied automatically from 10 s^{-1} down to 0.01 s^{-1}. The static yield stress was determined by the intercept at zero shear rate. The second approach rules out particle jamming as the mechanism for the observed large yield stress. The two approaches yielded almost identical results. The experimental values represent the arithmetic means of the two approaches. A specially designed tensile device was used to measure the Young's modulus of the high-field solid state during the pulling process, where the GER colloid was sandwiched between two parallel electrodes, with the upper one vertically movable and connected to a tensile meter. The dielectric constant was measured by an LCR meter (HP 4192) at 10 Hz with an electric field of 1 V mm^{-1}. As the dielectric constant is a monotonically decreasing function of frequency, the value at 10 Hz may be regarded as the lower bound to the d.c. value. A digital current meter monitored the conduction current (imaginary part of the dielectric constant). The GER response time was measured by a device previously reported[27].

NUMERICAL SIMULATIONS

The electrostatic energy is given by[28]

$$W_{es} = -\frac{1}{8\pi}\int_{V_0} \mathbf{D}\cdot\mathbf{E}\,\mathrm{d}V - \frac{1}{4\pi}\int_{V_S}\mathrm{d}V\int_0^{\mathbf{E}}\mathbf{D}\cdot\delta\mathbf{E}$$

$$= -\frac{1}{8\pi}\int_{V_0}\mathbf{D}\cdot\mathbf{E}\,\mathrm{d}V - \frac{1}{8\pi}\int_{V_S}E^2\,\mathrm{d}V - \frac{1}{2}\int_{V_S}\mathbf{P}\cdot\mathbf{E}\,\mathrm{d}V - \frac{1}{2}\,H(\mathbf{E}-\mathbf{E}_c)\int_{V_S}(\mathbf{E}-\mathbf{E}_c)\cdot\mathbf{P}\,\mathrm{d}V \quad (1)$$

where V_s is the volume of the saturation dipole layers in the contact region, and V_0 is the volume outside the dipole layers. The two parts require separate treatment because of the nonlinear P–E relation inside V_s. Here the step function $H(\mathbf{E}-\mathbf{E}_c) = 1$ if $|\mathbf{E}| > |\mathbf{E}_c|$ and zero otherwise, where $\mathbf{E}_c$ refers to the field inside the dipole layer when the applied field is ~60 V mm^{-1}, observed to be the field at which the particles start to aggregate, leading to the saturation surface polarization. $\mathbf{D} = \mathbf{E} + 4\pi\mathbf{P}(\mathbf{E})$, $\mathbf{E} = -\nabla\varphi$, and the P–E curve is modelled to consist of two segments: $\mathbf{P} = \mathbf{P}_0$ if $|\mathbf{E}| > |\mathbf{E}_c|$, otherwise $\mathbf{P} \propto \mathbf{E}$. We used the finite element approach to solve the Laplace equation $\nabla\varepsilon(\mathbf{x})\nabla\varphi = 0$, where $\mathbf{x}$ is the position vector, for the electrostatic potential φ everywhere in our model. About 500,000 tetrahedron elements were used, with the smallest ones in the elastic contact region extending 0.1 nm in each direction. The potentials were fixed as φ_+ and φ_- on the z boundaries (applied field $E = (\varphi_+ - \varphi_-)/L$, where L is the length of the sample, about two sphere diameters), and periodicity along the x and y directions was imposed. The dipoles were modelled by two localized charge densities separated by a fixed distance of 0.2 nm. Each dipole occupies a cube with a volume of 0.1 nm^3. The calculated $\Delta W_{es} > 0$ arises mainly from the smaller contact area with

increasing θ (and a larger centre-to-centre separation). The elastic deformation energy W_{elas} is given by[21] $W_{elas} = [\sqrt{(2R)}/5\kappa](\Delta L)^{5/2}$.

Received 2 July 2003; accepted 1 September 2003; published 5 October 2003.

References

1. Whittle, M. & Bullough, W. A. The structure of smart fluids. *Nature* **358,** 373–373 (1992).
2. Halsey, T. C. Electrorheological fluids. *Science* **258,** 761–766 (1992).
3. Clercx, H. & Bossis, G. Many-body electrostatic interaction in electrorheological fluids. *Phys. Rev. E* **48,** 2721–2738 (1993).
4. Tao, R. & Sun, J. M. Three-dimensional structure of induced electrorheological solid. *Phys. Rev. Lett.* **67,** 398–401 (1991).
5. Gamota, D. R. & Filisko, F. E. Linear and nonlinear mechanical-properties of electrorheological materials. *Int. J. Mod. Phys B* **6,** 2595–2607 (1992).
6. Chen, Y., Sprecher, A. F. & Conrad, H. Electrostatic particle–particle interaction in electrorheological fluids. *J. Appl. Phys.* **70,** 6796–6803 (1991).
7. Davis, L. C. Ground-state of an electrorheological fluid. *Phys. Rev. A* **46,** R719–R721 (1992).
8. Martin, J. E., Odinek, J., Halsey, T. C. & Kamien, R. Structure and dynamics of electrorheological fluids. *Phys. Rev. E* **57,** 756–775 (1998).
9. Anderson, R. A. in *Electrorheological Fluids* (ed. Tao, R.) 81–90 (World Scientific, Singapore, 1992).
10. Davis, L. C. Polarization forces and conductivity effects in electrorheological fluids. *J. Appl. Phys.* **74,** 1334–1340 (1992).
11. Garino, T., Adolf, D. & Hance, B. in *Electrorheological Fluids* (ed. Tao, R.) 167–174 (World Scientific, Singapore, 1992).
12. Randall, C. A., McCauley, D. E., Bowen, C. P., Shrout, T. R. & Messing, G. L. in *Electrorheological Fluids* (eds Tao, R. & Roy, G. D.) 60–66 (World Scientific, Singapore, 1994).
13. Liang, R. & Xu, Y. in *Electrorheological Fluids* (eds Tao, R. & Roy, G. D.) 233–250 (World Scientific, Singapore, 1994).
14. Randall, C. A., Bowen, C. P., Shrout, T. R., Messing, G. L. & Newnham, R. E. in *Electrorheological Fluids* (eds Tao, R. & Roy, G. D.) 516–525 (World Scientific, Singapore, 1994).
15. Ma, H. R., Wen, W., Tam, W. Y. & Sheng, P. Frequency dependent electrorheological properties: origin and bounds. *Phys. Rev. Lett.* **77,** 2499–2502 (1996).
16. Tam, W. Y. *et al.* New electrorheological fluid: theory and experiment. *Phys. Rev. Lett.* **78,** 2987–2990 (1997).
17. *Handbook of Chemistry and Physics* 62nd edn (eds Weast, R. C. & Astle, M. J.) (CRC, Boca Raton, 1981–1982).
18. Ma, H., Wen, W., Tam, W. Y. & Sheng, P. Dielectric electrorheological fluids: theory and experiment. *Adv. Phys.* **52,** 343–383 (2003).
19. Atten, P., Foulc, J.–N. & Felici, N. A conduction model of the electrorheological effect. *Int. J. Mod. Phys. B* **8,** 2731–2745 (1994).
20. Davis, L. C. & Ginder, J. M. in *Progress in Electrorheology* (eds Havelka, K. O. & Filisko, F. E.) 107–114 (Plenum, New York, 1995).
21. Landau, L. D. & Lifshitz, E. M. *Theory of Elasticity* 3rd edn (Pergamon, Oxford, 1986).
22. Neugebauer, C. A. & Webb, M. B. Electrical conduction mechanism in ultrathin, evaporated metal films. *J. Appl. Phys.* **33,** 74–82 (1962).
23. Hill, R. M., Electrical conduction in ultra thin metal films. I. Theoretical. *Proc. R. Soc. Lond. A* **309,** 377–395 (1969).
24. *Proc. 8th Int. Conf. Electrorheological Fluids and Magnetorheological Suspensions* (ed. Bossis, G.) (World Scientific, Singapore, 2002).
25. Clark, I. J., Takeuchi, T., Ohtori, N. & Sinclair, D. C. Hydrothermal synthesis and characterization of $BaTiO_3$ fine powders: precursors, polymorphism and properties. *J. Mater. Chem.* **9,** 83–91 (1999).
26. Xu, H. & Gao, L. New evidence of a dissolution-precipitation mechanism in hydrothermal synthesis of barium titanate powders. *Mater. Lett.* **57,** 490–494 (2002).
27. Wen, W., Zheng, D. & Tu, K. Experimental investigation for the time-dependent effect in electrorheological fluids under time-regulated high pulse electric field. *Rev. Sci. Instrum.* **69,** 3573–3576 (1998).
28. Jackson, J. D. *Classical Electrodynamics* 2nd edn (Wiley, New York, 1975).

Acknowledgements

This research was partially supported by CERG HKUST6065/02P and NSFC No.10029401. We thank Y. Zheng for help in TEM pictures. W.W. and P.S. also thank C. T. Chan and W. K. Ge for support. Correspondence and requests for materials should be addressed to P.S.

Competing financial interests

The authors declare that they have no competing financial interests.